

See discussions, stats, and author profiles for this publication at: <https://www.researchgate.net/publication/327191391>

# Investigating LINC Complex Protein Homo-oligomerization in the Nuclear Envelopes of Living Cells Using Fluorescence Fluctuation Spectroscopy: Methods and Protocols

Chapter in *Methods in molecular biology* (Clifton, N.J.) · August 2018

DOI: 10.1007/978-1-4939-8691-0\_11

CITATIONS

8

READS

55

5 authors, including:



**Kwang Ho Hur**

University of Minnesota Twin Cities

23 PUBLICATIONS 77 CITATIONS

SEE PROFILE



**Gw Gant Luxton**

University of California, Davis

61 PUBLICATIONS 1,637 CITATIONS

SEE PROFILE

Some of the authors of this publication are also working on these related projects:



Mechanotransduction [View project](#)



Herpesvirus capsid transport [View project](#)

**Investigating LINC complex protein homo-oligomerization in the nuclear envelopes of living cells using fluorescence fluctuation spectroscopy**

Jared Hennen<sup>1</sup>, Isaac Angert<sup>1</sup>, Kwang-Ho Hur<sup>1</sup>, G.W. Gant Luxton<sup>2\*</sup>, and Joachim D. Mueller<sup>1</sup>□

<sup>1</sup>School of Physics and Astronomy, University of Minnesota, Minneapolis, MN 55455

<sup>2</sup>Department of Genetics, Cell Biology, and Development, University of Minnesota, Minneapolis, MN 55455

□ Signifies co-corresponding authors

**Corresponding author info:**

G.W. Gant Luxton\*

Room 6-160 Jackson Hall

321 Church St SE

Minneapolis, MN 55455

Phone: (612)-624-8343

Fax: (612)-626-6140

[gwgl@umn.edu](mailto:gwgl@umn.edu)

Joachim D. Mueller

PAN 418

115 Union St SE

Minneapolis, MN 55455

Phone: (612)-625-4369

Fax: (612)-624-7375

[mueller@physics.umn.edu](mailto:mueller@physics.umn.edu)

## Summary

Linker of nucleoskeleton and cytoskeleton (LINC) complexes are conserved nuclear envelope (NE) spanning molecular bridges which mechanically integrate the nucleus with the cytoskeleton and mediate force transmission into the nucleoplasm. Despite their critical roles in fundamental cellular processes such as meiotic chromosome and nuclear positioning, the mechanism of LINC complex assembly in cells remains unclear. To begin to address this deficit, we recently developed z-scan fluorescence fluctuation spectroscopy (FFS) and brightness analysis as a method for quantifying the oligomeric states of fluorescent protein-tagged NE proteins including nesprins and SUN proteins. Since the homo-oligomerization of SUN2 is critical for its ability to interact with nesprins within the perinuclear space, the knowledge obtained through quantitative brightness experiments reveals important insights into the *in vivo* mechanisms of LINC complex assembly. Here we describe the procedure we use to determine the brightness of proteins in the NE of living cells. In addition to the measurement procedure, we discuss the instrumentation requirements and present the results of applying this procedure to measure the brightness of nesprin-2 and SUN2.

### Key words:

Brightness, FFS, KASH, LINC complex, nesprin, nuclear envelope, perinuclear space, SUN protein

## 1. Introduction

LINC complexes span the NE and physically couple chromatin and the nucleoskeleton with the cytoskeleton (1). These conserved mechanosensitive molecular bridges are essential for the transmission of mechanical stimuli from the extracellular matrix through the cytoskeleton and into the nuclear interior (2, 3). Consequently, LINC complex-mediated mechanotransmission is required for several fundamental cellular processes such as meiotic chromosome pairing, mechanotransduction, and nuclear positioning (4, 5). Further highlighting their central importance in cellular mechanobiology is a growing list of genetic mutations in LINC complex proteins that are associated with a myriad of human diseases including cancer, hearing loss, and muscular dystrophy (4, 6).

LINC complexes consist of the outer and inner nuclear membrane *Klarsicht/ANC-1/SYNE* homology (KASH) and *Sad1/UNC-84* (SUN) proteins, respectively (7). KASH proteins are identified by their conserved C-terminal KASH domain, which contains a transmembrane domain followed by the luminal ~10-32 residue KASH peptide (8). The divergent spectrin repeat-containing N-termini of KASH proteins project away from the nucleus into the cytoplasm where they interact with the cytoskeleton (4). SUN proteins directly interact with KASH-peptides within the perinuclear space via their conserved and eponymous C-terminal SUN domain (9, 10). Within the nucleoplasm, the divergent N-termini of SUN proteins engage A-type lamins, chromatin, and other inner nuclear membrane proteins (11). Mammals encode six KASH proteins (nesprins-1-4, lymphocyte-restricted membrane protein (LRMP), and KASH5) and five SUN proteins (SUN1-5) (5).

Several recent *in vitro* studies have provided invaluable structural insights into the SUN-KASH interaction and the ability of LINC complexes to transmit mechanical forces. Specifically, SUN2 homo-trimerization was demonstrated to be a prerequisite for KASH-binding and an intermolecular disulfide bond was shown to exist between conserved cysteine residues in the SUN domain and KASH peptides of nesprin-1 and -2 (**12–14**). Notwithstanding these significant advances, key questions remain. For example, do SUN2 homo-trimers exist in the NE of living cells? Do all SUN proteins homo-trimerize in order to interact with KASH proteins? How is the SUN-KASH interaction regulated?

To begin to address these questions, we recently extended the application of FFS to quantify protein-protein interactions in the NE in living cells (**15, 16**). The procedure outlined here can be used to measure the number concentration and brightness of LINC complex components, as well as other NE proteins, within their native environment. The brightness  $\lambda$  recovered from an FFS measurement represents the mean photon count rate of a fluorescently labeled protein complex and is proportional to its average oligomeric state (**17**). To highlight this we determine the normalized brightness  $b$  where a monomeric protein would have  $b = 1$  while a trimeric protein would have  $b = 3$ . Here, we demonstrate how this approach has been used to determine the oligomeric state of the KASH peptide of nesprin-2 and the luminal domain of SUN2 in the NE of living U2OS cells.

## 2. Materials

### 2.1 FFS instrumentation

FFS experiments can be performed in cells using a research-grade confocal or multi-photon inverted microscope that is equipped with sensitive photon counting detectors (quantum efficiency > 40% in the wavelength region of interest). While many commercial microscope systems are suitable for FFS experiments, we will briefly describe our home-built two-photon (2P) microscope that we use for collecting FFS data from cells (see **Note 1**). This description of our custom 2P microscope should provide a useful resource for those investigators considering employing FFS in their research. A schematic of our instrumental setup is provided in Figure 1.

1. Zeiss Axiovert 200 microscope (Carl Zeiss AG, Jena, Germany) which is mounted on a research grade optical table (RS2000, Newport, Irvine, CA) supported by pneumatic isolators (S-2000A, Newport, Irvine, CA) for vibration isolation.
2. Mode-locked Ti:sapphire laser (Tsunami, Spectra Physics, Mountain View, CA) for 2P excitation. We prefer to use excitation wavelengths in the range of 900-1000 nm for measuring EGFP in living cells; here we chose a wavelength of 1000 nm.
3. Beam expander to achieve overfilling of the back aperture of the objective (see **Note 2**).
4. Two steering mirrors (10Q20UF.35S, Newport, Irvine, CA) to align the laser beam into the beam expander (see **Note 3**).

5. Multi-photon short-pass dichroic beam-splitter (675DCSXR, Chroma Technology, Bellows Falls, VT) to separate the excitation light from the emitted fluorescence.
6. Short-pass barrier filter (FF01-750/SP-25, Semrock, Rochester, NY) to remove any residual scattered laser light.
7. Zeiss 63x C-Apochromat water immersion objective with NA = 1.2 (see **Note 4**) to focus the excitation light into the sample.
8. PZ-2000 XYZ series automated stage with a piezo z-axis top plate (ASI, Eugene, OR) fitted on the microscope stage for performing z-scan measurements in cells.
9. 30 MHz 33522A Function/Arbitrary waveform generator (Agilent Technologies, Santa Clara, CA) to drive the z-axis piezo controller via an external analog input.
10. SPCM-AQ-141 single-photon counting module (Perkin-Elmer, Dumberry, Quebec) which is mounted on an XYZ linear translation stage (562-XYZ, Newport, Irvine, CA) for alignment and produces transistor-transistor logic (TTL) pulses that are recorded by a Flex04-12D data acquisition card (correlator.com, Bridgewater, NJ) and stored in computer memory for subsequent analysis.

## 2.2 Samples and microscope slide

1. 24-well glass-bottom slide with #1.5H cover glass (In Vitro Scientific, Sunnyvale, CA) (see **Note 5**).
2. The 24-well should contain the following in separate wells but on the same 24-well plate (see **Note 6**):
  - a) Texas Red at 200 nM or other standard fluorescent dye-solution.
  - b) U2OS cells transiently transfected with EGFP (see **Note 7**).
  - c) U2OS cells transiently transfected with tandem dimeric EGFP (EGFP<sub>2</sub>).
  - d) U2OS cells transiently transfected with SS-EGFP.
  - e) U2OS cells transiently transfected with other EGFP-tagged NE proteins of interest.

## 3. Methods

### 3.1 Optimize collar position of objective

1. Focus the excitation beam ~40  $\mu\text{m}$  above the glass-solution interface in the dye solution.
2. Record photon counts for ~60 seconds at a sampling rate of 100 kHz for dye measurements.
3. Analyze the photon counts using a standard algorithm (**18**) to obtain the brightness  $\lambda$  in units of counts per second.
4. Systematically adjust the collar and measure the brightness of the dye to determine the collar position that maximizes the brightness (Figure 2A). The resulting resolution in collar position is typically +/- 2  $\mu\text{m}$ .
5. If the measured brightness of the dye solution is independent of focal depth (Figure 2B), the position of the correction collar has been successfully verified.

### 3.2 Select an appropriate excitation power.

1. Identify an EGFP-expressing cell that has a uniform distribution of cytoplasmic fluorescence using epifluorescence.
2. Use bright field illumination to identify an area of the cytoplasm in the cell identified in Step 1 that lacks obvious large organelles.
3. Aim and focus the laser in the cytoplasmic area identified in Step 2 so as to maximize the intensity of the detected fluorescence signal.
4. Collect photon counts for ~10 seconds to determine the mean intensity.
5. Adjust the laser power and repeat step 4.
6. Plot fluorescence intensity vs. the squared power. There should be a linear increase at low powers with deviation from linearity at higher powers due to photobleaching and excitation saturation (Figure 3A) (see **Note 8**).
7. Brightness measurements must be taken in the regime where intensity scales linearly with the squared power (solid red line, Figure 3A). Typically, we conservatively set the excitation power to  $\sim 1/5^{\text{th}}$  of the maximum power of the linear regime for brightness experiments.
8. The limiting excitation power should be experimentally determined for every fluorescently labeled protein to verify that the chosen power is still in the linear power regime. Once the excitation power is chosen, it must be kept constant throughout all subsequent experiments to ensure a fixed brightness value of EGFP.

### 3.3 Measure the reference brightness of EGFP in living cells.

1. Choose a cell, then position and focus the laser as in steps 1-3 in section 3.2.
2. Collect FFS data from the focused beam at this cytoplasmic location for ~60 seconds with a 20 kHz acquisition rate.
3. Perform a z-scan (Figure 3B) through the cell at this cytoplasmic location at a rate of  $\sim 5 \mu\text{m/s}$  with a peak-to-peak amplitude of  $\sim 20 \mu\text{m}$ .
  - a. The z-scan intensity data (Figure 3C) along with the data collected in step 4 are analyzed as previously described to determine the brightness  $\lambda$  and the number concentration  $N$  of the sample (**19**).
  - b.  $N$  represents the average number of EGFP monomers within the point spread function (PSF) and is calculated by dividing the mean intensity  $\langle F \rangle$  by the reference brightness,  $N = \langle F \rangle / \lambda_{EGFP}$ . If the PSF volume is known, the number concentration can be converted to a molar concentration as described elsewhere (**16**).
4. Repeat steps 1-3 for a minimum of 10 cells with varied expression levels of EGFP.
  - a. The resulting brightness values should be concentration independent to within a relative standard deviation  $\leq 10\%$  (Figure 3D).
  - b. The mean value defines the reference brightness  $\lambda_{EGFP}$ .

5. Repeat steps 1-4 for cells expressing EGFP<sub>2</sub>.
  - a. The resulting brightness should be twice the average brightness of EGFP (Figure 3D).
  - b. To emphasize the relationship between brightness and oligomeric state, we define the normalized brightness  $b$  as  $b = \lambda / \lambda_{EGFP}$  (**20**). Measurements of EGFP<sub>2</sub> should have an average  $b$  within ~10% of  $b = 2$  (see **Note 9**).

### 3.4 Brightness measurement of EGFP in the NE.

The procedure we use for measuring brightness in the NE is similar to the one used to measure brightness in the cytoplasm. However, we have found the NE to be much more challenging experimentally. Consequently, brightness measurements in the NE require additional precautions as we describe below. The following experimental procedure demonstrates how to measure the brightness of EGFP that is targeted to the endoplasmic reticulum lumen and the contiguous perinuclear space of the NE by fusing the signal sequence (SS) of the luminal protein torsinA to the N-terminus of EGFP (SS-EGFP) (**16, 21**). Measurements of EGFP in the NE serve as a control and a result of  $b = 1$  establishes the fidelity of brightness analysis in the NE.

1. Use epifluorescence to identify an SS-EGFP-expressing cell that displays a clear and distinct ring of fluorescence around the nucleus (Figure 4A).
2. Switch to bright-field illumination and identify a location within the center of the nucleus from the cell identified in Step 1 that is devoid of visible structures (i.e. nucleoli) (Figure 4A) (see **Note 10**).
3. Perform a z-scan at the location identified in Step 2 (Figure 4B).
4. Fit the z-scan intensity data generated in Step 3 using the procedure described in Smith et al (**22**).
  - a. The fit identifies the fluorescence contributions from the ventral and dorsal NEs as well as the background signal originating from sources outside the NE (Figure 4C).
  - b. Analysis further determines the intensity fraction of the fluorescence contributions from each NE. Only cells with an NE intensity fraction  $\geq 0.9$  are selected for brightness measurements. This criterion ensures that contributions from the background signal are at most 10%, which represents a negligible amount for brightness analysis (**16**). The remaining steps are performed only with cells that satisfy this criterion.
5. Focus the PSF on the ventral NE by maximizing the collected fluorescence intensity.
6. Collect ~60 s of data with a 20 kHz data acquisition rate (Figure 4D).
  - a. Plot the intensity averaged over 1 s vs. time (Figure 5).
  - b. Data showing no significant change in the average intensity (Figure 5A) can be used for further analysis. Data containing a peak-to-peak difference exceeding 20% of the mean in the averaged intensity (Figure 5B) should be discarded and retaken (see **Note 11**).
  - c. If it is difficult to obtain data without sudden changes in intensity, we have found that moving to a different location within the cell tends to result in stable data.

7. Determine the brightness of SS-EGFP from the data taken in Step 6 using the analysis procedure described in Hennen et al (**16**).
8. Repeat Steps 5-7 in the dorsal NE.
9. Collect a final z-scan.
  - a. The intensity traces of the initial and final z-scan are compared to ensure that no detectable changes occurred during the measurement process. Focus drift of the instrument or motion of the cell would lead to a mismatch between the z-scan intensity profiles. If a mismatch is detected, the data are discarded.
10. Repeat Steps 1-9 for at least 10 cells.
  - a. Select cells that vary in expression level to obtain the brightness over a wide range of concentrations. A plot of the normalized brightness of SS-EGFP vs. number concentration is shown in Figure 6. The experimental brightness is independent of concentration and has an average value of  $0.99 \pm 0.06$ . This result is consistent with SS-EGFP being a monomer, as expected. It is important to check that SS-EGFP can be accurately measured as a monomer before attempting to measure functional proteins in the NE.

### 3.5 Measuring the oligomerization of LINC complex constituents in the NE.

The procedure described above in section 3.4 can also be used to measure the brightness of EGFP-tagged proteins in the NE; therefore, in the following section we will demonstrate its application to the study of the molecular mechanisms underlying LINC complex assembly. To do this, we will describe how to measure the brightness of EGFP-tagged mouse nesprin-2 and SUN2 in the NE.

1. The technique described here requires the proteins being measured to diffuse in order to observe intensity fluctuations. Since both EGFP-tagged mini-nesprin-2G, a functional nesprin-2G construct (**23**), and full-length SUN2 are highly immobile in the NE (**24**), they are rapidly photobleached by 2P excitation and therefore unsuitable for standard quantitative brightness experiments. For this reason, we limit our analyses here to the luminal domain of each protein, which is targeted to the perinuclear space of the NE by an N-terminal SS-EGFP fusion (SS-EGFP-KASH2 and SS-EGFP-SUN2<sup>261-731</sup>) (**16**).
2. Perform the same procedure described in section 3.2 for each protein being measured. While mobile, functional proteins such as SS-EGFP-SUN2<sup>261-731</sup> may have lower mobility than the calibration proteins discussed in previous sections (**16**). Proper excitation power should be determined prior to measuring the reference brightness.
3. Measure the  $b$  of the proteins of interest following the procedure described above in Section 3.4.
  - a. Measurements of SS-EGFP-KASH2 showed no change in  $b$  over the range of measured  $N$ , with an average of  $b = 1.05 \pm 0.1$  consistent with a monomer (Figure 7A).
  - b. Measurements of SS-EGFP-SUN2<sup>261-731</sup> showed  $b$  increased in an  $N$ -dependent manner and approached a limiting value of  $b = 3$  (Figure 7B).

4. The brightness curve for SS-EGFP-SUN2<sup>261-731</sup> shown in Figure 7B represents a binding titration. These measurements are performed in the presence of endogenous non-labeled SUN2, which may complicate the interpretation of this curve (see **Note 12**). Nevertheless, the effect of endogenous binding competition becomes negligible once the concentration of the exogenous labeled protein significantly exceeds that of the endogenous protein. In this regime, the  $b$  curve should asymptotically approach a limiting value which corresponds to the limiting oligomeric state of the protein. Consequently, the saturating brightness value of  $b = 3$  reached at high concentrations of SS-EGFP-SUN2<sup>261-731</sup> reflects the limiting oligomeric state of the protein.
5. Repeat brightness experiments over several days on new cell preparations to ensure that the results obtained are both robust and reproducible. In addition to ensuring the reproducibility of the results, this generates a sufficient number of data points so that a reasonably dense  $b$  curve can be constructed. A single experiment will typically consist of  $b$  measurements performed in 15 cells after accounting for the calibrations, reference measurements, and analysis criteria described above. The data shown in Figures 7A and 7B represent 2 and 6 separate experiments, respectively.

## NOTES

1. We prefer 2P excitation to one-photon confocal microscopy for FFS because it reduces the levels of out-of-focus photobleaching and phototoxicity experienced in living cells (**25, 26**). In addition, the absence of the confocal pinhole in a 2P microscope results in a less complicated optical system, which facilitates instrument alignment and simplifies ongoing maintenance. Moreover, 2P excitation generates an excitation volume, or PSF, that can be accurately described by heuristic analytical functions such as the modified Gaussian-Lorentzian model (**19**). Such knowledge regarding the nature of the PSF is essential for the successful execution of the quantitative FFS method described here.
2. A typical value for the excitation beam overfill factor is  $2\omega_0/D \sim 2$ , where  $\omega_0$  and  $D$  are the radial beam waist and the pupil diameter of the objective, respectively. Before initiating a quantitative FFS experiment, it is essential that the excitation beam be properly aligned such that it passes through the center of the objective and the detector. Stable experimental setups will require minimal beam alignment adjustments from day to day. Established, instrument-specific procedures should be followed to ensure that the beam is correctly aligned.
3. While inexpensive dielectric mirrors offer excellent reflectivity, only metallic mirrors or dielectric mirrors specially designed for femtosecond pulsed lasers should be used. This choice will minimize the reduction of the peak power of the laser due to group velocity dispersion (**27**).
4. The choice of objective is of utmost importance when designing an FFS system, as the signal-to-noise ratio of FFS experiments is highly dependent upon the efficient collection of fluorescence from individual molecules. Since the 2P excitation efficiency is proportional to the fourth power of the NA of the objective, FFS experiments performed in cells require the use of high NA objectives ( $NA > 1$ ) (**25**). We find C-Apochromat water-immersion objectives with a correction collar to compensate for variations in coverslip thickness to be the

most suitable for collecting FFS data from cells. We discourage the use of oil-immersion objects because they introduce spherical aberrations, which complicate the interpretation of FFS experiments **(28)**.

5. While the nominal thickness of standard #1.5 cover glass is 0.17 mm, actual thicknesses may vary between 0.16 and 0.19 mm. These deviations in thickness are a major source of spherical aberrations for high NA objectives. Such aberrations alter the size and shape of the focused excitation beam as a function of focal depth and lead to biased FFS data **(29)**. Therefore, the use of a high NA water-immersion objective equipped with a correction collar designed to compensate for the actual cover glass thickness is imperative for quantitative FFS experiments. Although we use a micrometer to directly measure the thickness of our cover glasses, we find that in practice the optimal collar position for FFS differs from the values printed on the objective collar by a constant offset, which is unique to each objective. Whenever possible, we recommend the use of #1.5H cover glass, which has a tighter tolerance ( $0.170 \pm 0.005$  mm) than regular #1.5 slides. The consistency in cover glass thickness minimizes the range of collar positions that must be tested when changing slides.

6. All of the experiments must be done in the same 24-well glass bottom slide in order to take advantage of the procedure described in section 3.1. This procedure must be repeated for every new 24-well glass bottom slide used.

7. For the experiments described here, we used the human osteosarcoma U2OS cell line grown in Dulbecco's modified Eagle's medium supplemented with 10% fetal bovine serum. The cells are plated in wells and transiently transfected with the relevant cDNA constructs. Finally, the cell growth media is exchanged for phosphate buffered saline immediately before the start of measurement.

8. Quantitative  $b$  measurements in cells necessitate the selection of an appropriate excitation power to minimize photobleaching and excitation saturation **(30)**. The presence of either photobleaching or excitation saturation bias the interpretation of FFS data, which further complicates the analysis **(31, 32)**.

9. Measurements of EGFP<sub>2</sub> are required in order to validate that the system is behaving as expected. Brightness values significantly above or below  $b = 2$  are indicative of issues that complicate the interpretation of FFS measurements of the proteins of interest.

10. We avoid performing measurements near the edge of the nucleus as these areas of the NE may have significant curvature.

11. All fluorescence fluctuation methods implicitly assume a stationary signal that remains constant throughout the measurement period **(33)**. While the intensity is typically stable for measurements performed in the cytoplasm, we have found a higher fraction of measurements in the NE with unstable intensities. Data containing large changes in the average intensity are not conducive to our analysis.

12. An approximate measure of the effective dissociation coefficient is given by  $N$  where the brightness is halfway between its minimum and maximum value. However, since the data were taken in the presence of endogenous SUN2, binding competition between endogenous protein and SS-EGFP-SUN2<sup>261-731</sup> could lead to complexes containing a mixture of labeled and unlabeled protein, which reduce the observed  $b$ . The net effect of this competition is a shift of the brightness curve to higher  $N$ . Thus, the estimated dissociation coefficient provides an upper limit of the true value. Depleting the endogenous protein using methods such as RNA

interference or genetic knockout will remove endogenous competition, thereby allowing measurement of the true binding affinity.

## **ACKNOWLEDGMENTS**

This work was financially supported in part by the NIH (JDM (GM064589), and CAS (AR007612)), and the Dystonia Medical Research Foundation (GWGL and JDM).

## **ABBREVIATIONS**

<i>b</i>	Normalized brightness
KASH:	<i>Klarsicht</i> , <i>ANC-1</i> , SYNE homology
LINC:	Linker of nucleoskeleton and cytoskeleton
<i>N</i> :	Number concentration
NE:	Nuclear envelope
SUN:	<i>Sad1/UNC-84</i>

## REFERENCES

1. Starr DA and Fridolfsson HN (2010) Interactions between nuclei and the cytoskeleton are mediated by SUN-KASH nuclear-envelope bridges. *Annu Rev Cell Dev Biol* 26:421–444
2. Alam S, Lovett DB, Dickinson RB, et al (2014) Nuclear forces and cell mechanosensing. *Prog Mol Biol Transl Sci* 126:205–215
3. Kaminski A, Fedorchak GR, and Lammerding J (2014) The cellular mastermind(?) – Mechanotransduction and the nucleus. *Prog Mol Biol Transl Sci* 126:157–203
4. Luxton GWG and Starr DA (2014) KASHing up with the nucleus: novel functional roles of KASH proteins at the cytoplasmic surface of the nucleus. *Curr Opin Cell Biol* 28:69–75
5. Meinke P and Schirmer EC (2015) LINC'ing form and function at the nuclear envelope. *FEBS Lett* 589:2514–2521
6. Horn HF (2014) LINC complex proteins in development and disease. *Curr Top Dev Biol* 109:287–321
7. Crisp M, Liu Q, Roux K, et al (2006) Coupling of the nucleus and cytoplasm: role of the LINC complex. *J Cell Biol* 172:41–53
8. Starr DA and Han M (2002) Role of ANC-1 in tethering nuclei to the actin cytoskeleton. *Science* 298:406–409
9. Malone CJ, Fixsen WD, Horvitz HR, et al (1999) UNC-84 localizes to the nuclear envelope and is required for nuclear migration and anchoring during *C. elegans* development. *Dev Camb Engl* 126:3171–3181
10. Kim DI, Birendra KC, and Roux KJ (2015) Making the LINC: SUN and KASH protein interactions. *Biol Chem* 396:295–310
11. Chang W, Worman HJ, and Gundersen GG (2015) Accessorizing and anchoring the LINC complex for multifunctionality. *J Cell Biol* 208:11–22
12. Sosa BA, Rothballer A, Kutay U, et al (2012) LINC complexes form by binding of three KASH peptides to domain interfaces of trimeric SUN proteins. *Cell* 149:1035–1047
13. Zhou Z, Du X, Cai Z, et al (2012) Structure of Sad1-UNC84 homology (SUN) domain defines features of molecular bridge in nuclear envelope. *J Biol Chem* 287:5317–5326
14. Wang W, Shi Z, Jiao S, et al (2012) Structural insights into SUN-KASH complexes across the nuclear envelope. *Cell Res* 22:1440–1452
15. Slaughter BD and Li R (2010) Toward Quantitative “In Vivo Biochemistry” with Fluorescence Fluctuation Spectroscopy. *Mol Biol Cell* 21:4306–4311
16. Hennen J, Hur K-H, Saunders CA, et al Quantitative Brightness Analysis of Protein Oligomerization in the Nuclear Envelope. *Biophys J* In press
17. Chen Y, Wei L-N, and Müller JD (2003) Probing protein oligomerization in living cells with fluorescence fluctuation spectroscopy. *Proc Natl Acad Sci U S A* 100:15492–15497
18. Sanchez-Andres A, Chen Y, and Müller JD (2005) Molecular brightness determined from a generalized form of Mandel's Q-parameter. *Biophys J* 89:3531–3547

19. Macdonald PJ, Chen Y, Wang X, et al (2010) Brightness Analysis by Z-Scan Fluorescence Fluctuation Spectroscopy for the Study of Protein Interactions within Living Cells. *Biophys J* 99:979–988
20. Chen Y and Müller JD (2007) Determining the stoichiometry of protein heterocomplexes in living cells with fluorescence fluctuation spectroscopy. *Proc Natl Acad Sci U S A* 104:3147–3152
21. Saunders CA, Harris NJ, Willey PT, et al (2017) TorsinA controls TAN line assembly and the retrograde flow of dorsal perinuclear actin cables during rearward nuclear movement. *J Cell Biol* 216:657–674
22. Smith EM, Hennen J, Chen Y, et al (2015) Z-scan fluorescence profile deconvolution of cytosolic and membrane-associated protein populations. *Anal Biochem* 480:11–20
23. Luxton GWG, Gomes ER, Folker ES, et al (2010) Linear arrays of nuclear envelope proteins harness retrograde actin flow for nuclear movement. *Science* 329:956–959
24. Ostlund C, Folker ES, Choi JC, et al (2009) Dynamics and molecular interactions of linker of nucleoskeleton and cytoskeleton (LINC) complex proteins. *J Cell Sci* 122:4099–4108
25. Denk W, Strickler JH, and Webb WW (1990) Two-photon laser scanning fluorescence microscopy. *Science* 248:73–76
26. Squirrell JM, Wokosin DL, White JG, et al (1999) Long-term two-photon fluorescence imaging of mammalian embryos without compromising viability. *Nat Biotechnol* 17:763–767
27. Guild JB, Xu C, and Webb WW (1997) Measurement of group delay dispersion of high numerical aperture objective lenses using two-photon excited fluorescence. *Appl Opt* 36:397–401
28. Gibson SF and Lanni F (1992) Experimental test of an analytical model of aberration in an oil-immersion objective lens used in three-dimensional light microscopy. *J Opt Soc Am A* 9:154–166
29. Nasse MJ and Woehl JC (2010) Realistic modeling of the illumination point spread function in confocal scanning optical microscopy. *J Opt Soc Am A Opt Image Sci Vis* 27:295–302
30. Patterson GH and Piston DW (2000) Photobleaching in Two-Photon Excitation Microscopy. *Biophys J* 78:2159–2162
31. Delon A, Usson Y, Derouard J, et al (2004) Photobleaching, mobility, and compartmentalisation: inferences in fluorescence correlation spectroscopy. *J Fluoresc* 14:255–267
32. Berland K and Shen G (2003) Excitation saturation in two-photon fluorescence correlation spectroscopy. *Appl Opt* 42:5566–5576
33. Hur K-H, Macdonald PJ, Berk S, et al (2014) Quantitative measurement of brightness from living cells in the presence of photodepletion. *PLoS One* 9:e97440

## FIGURE LEGENDS

**Figure 1. The FFS experimental set-up used in this work.**

**Figure 2. Calibration and verification of objective correction collar position.** (A) Brightness of Texas Red vs. water-immersion objective correction collar position. (B) Brightness of Texas Red vs. focal depth measured with a calibrated correction collar.

**Figure 3. Power calibration and brightness measurements of EGFP and EGFP<sub>2</sub> in the cytoplasm of living cells.** (A) Average fluorescence intensity vs. squared excitation power for EGFP expressed in U2OS cells. The solid red line is a linear fit to the data below 1.5 mW<sup>2</sup>, which is extended beyond the linear regime with the dashed red line. (B) Illustration of a z-scan through the cytoplasm of a cell expressing EGFP. (C) Intensity trace (black) and fit (white) of a z-scan through the cytoplasm of an EGFP expressing cell. (D) Plot of  $b$  vs.  $N$  for EGFP and EGFP<sub>2</sub> expressed in U2OS cells. The blue dashed line denotes the reference brightness  $\lambda_{EGFP}$ , while the red line denotes the value expected for a dimer.

**Figure 4. Performing brightness measurements in the NE of living cells.** (A) Illustration of a cell viewed via bright-field illumination. The NE is highlighted in green and nucleoli are shown in black. The red focus denotes a typical measurement position in the example cell. (B) Illustration of a z-scan with the excitation volume moving axially through the cell passing through the ventral and dorsal NE. (C) Intensity trace (black) of a z-scan through the nucleus of a SS-EGFP expressing cell with fit (solid white line). The fit is deconvolved to identify the contributions from the ventral NE (red squares), nucleoplasm (solid blue line), and dorsal NE (dashed green line). This analysis returned intensity fractions of 0.96 and 0.95 for the ventral and dorsal NE, respectively. (D) A 10-ms window of photon count data from a stationary measurement of SS-EGFP in the NE at full time resolution. The fluctuations encode information about the concentration and stoichiometry of labeled proteins.

**Figure 5. Intensity traces of SS-EGFP vs. time in the NE.** Intensity data were averaged over 1 s intervals. (A) Example of a stable intensity trace with no significant changes in the average intensity. (B) Example of an intensity trace containing a spike in the average intensity. This trace is not suitable for further analysis.

**Figure 6. Brightness of SS-EGFP in the NE.** Plot of  $b$  vs.  $N$  of SS-EGFP in the NE.

**Figure 7.  $b$  vs.  $N$  for LINC complex proteins in the NE.** Plots for (A) SS-EGFP-KASH2 and (B) SS-EGFP-SUN2<sup>261-731</sup>. Previously published in *Biophysical Journal* (16).

**FIGURE 1**

Arbitrary waveform

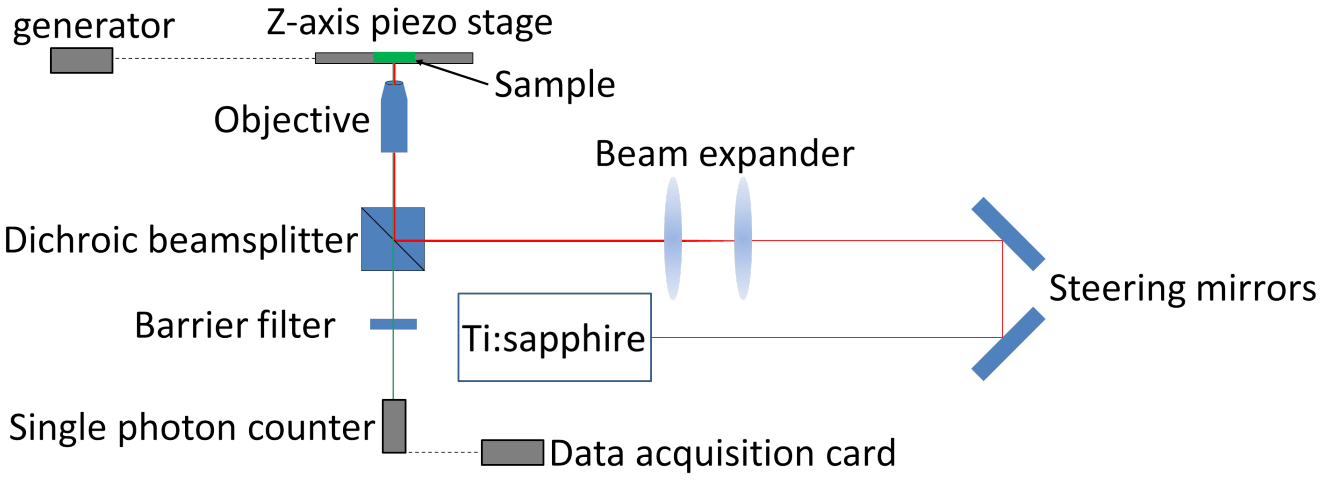


FIGURE 2

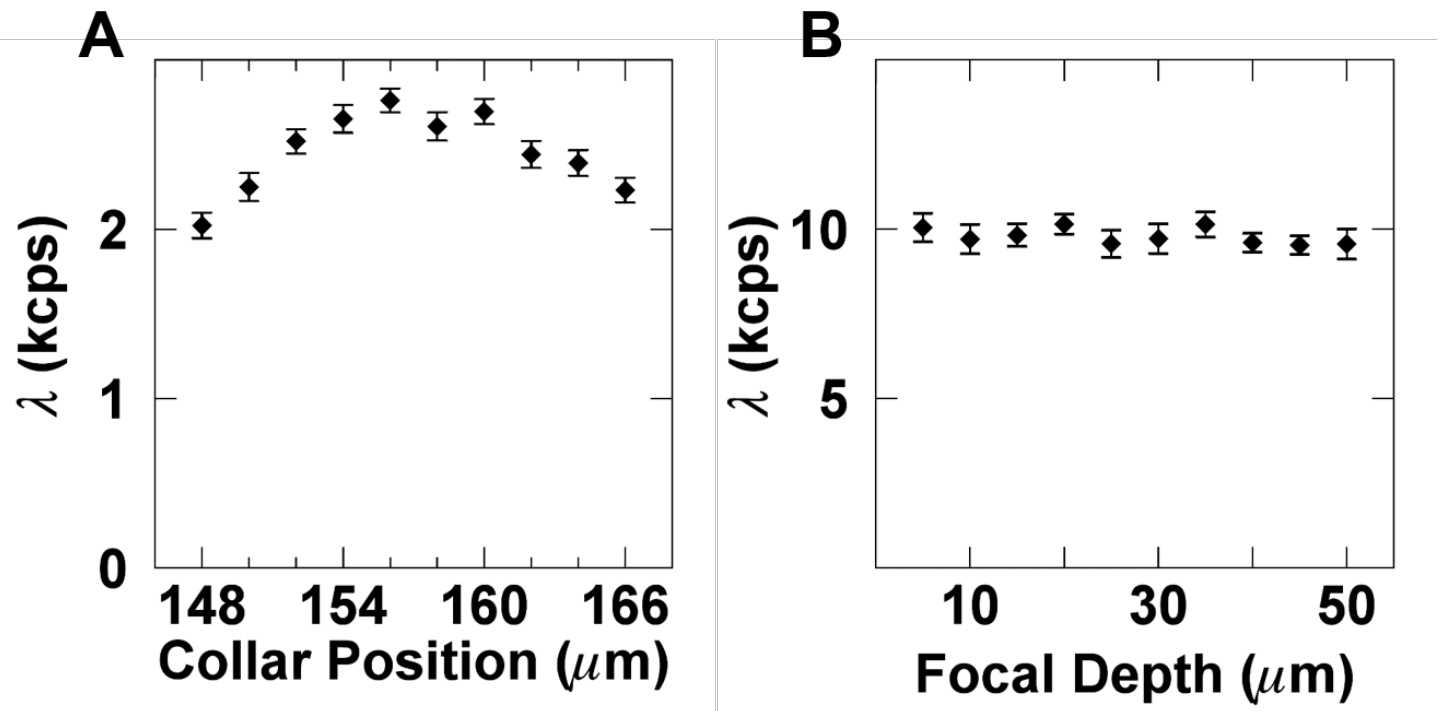


FIGURE 3

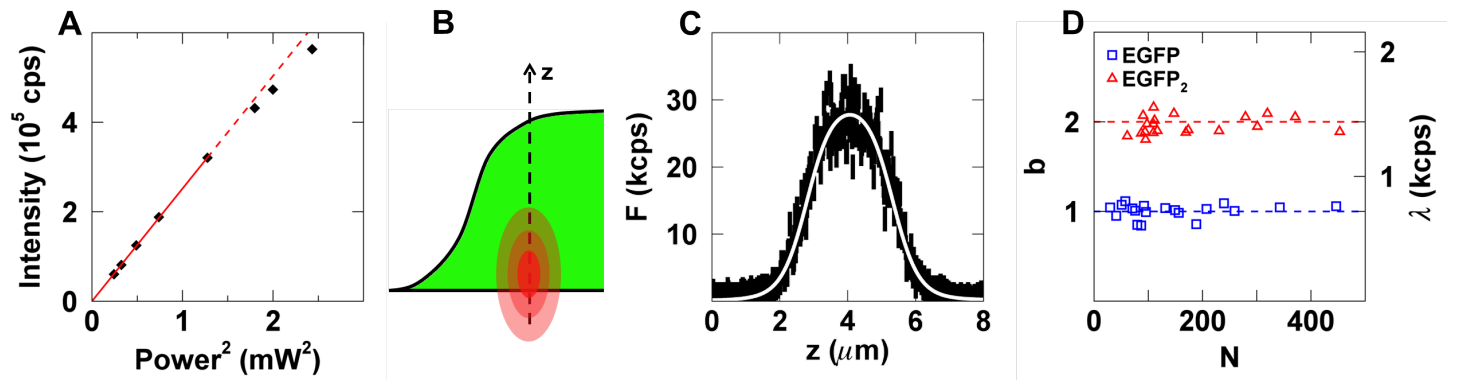
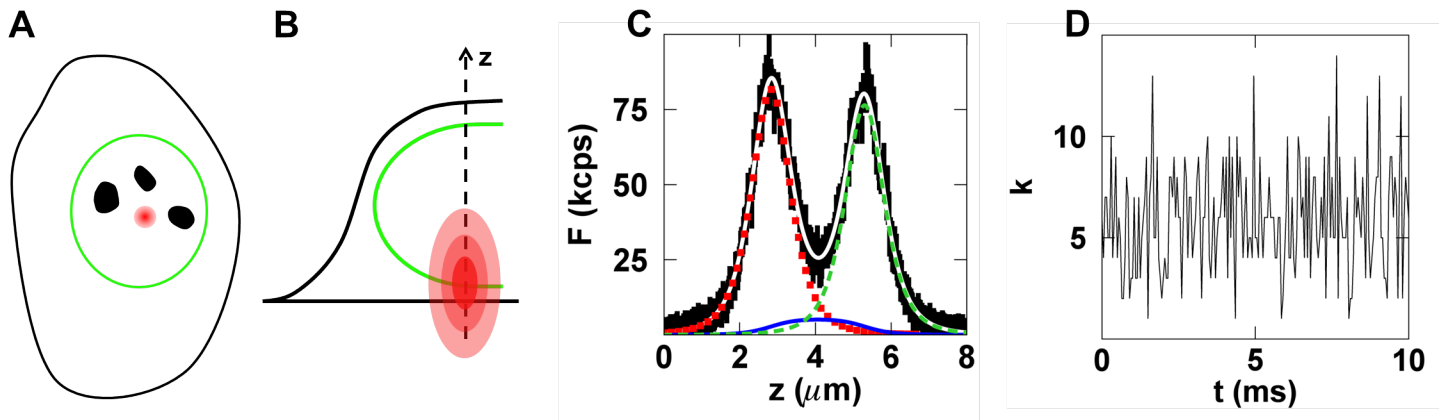


FIGURE 4



**FIGURE 5**

Figure 5 - Investigating LINC complex protein homo-oligomerization in the nuclear envelopes of living cells using fluorescence fluctuation spectroscopy

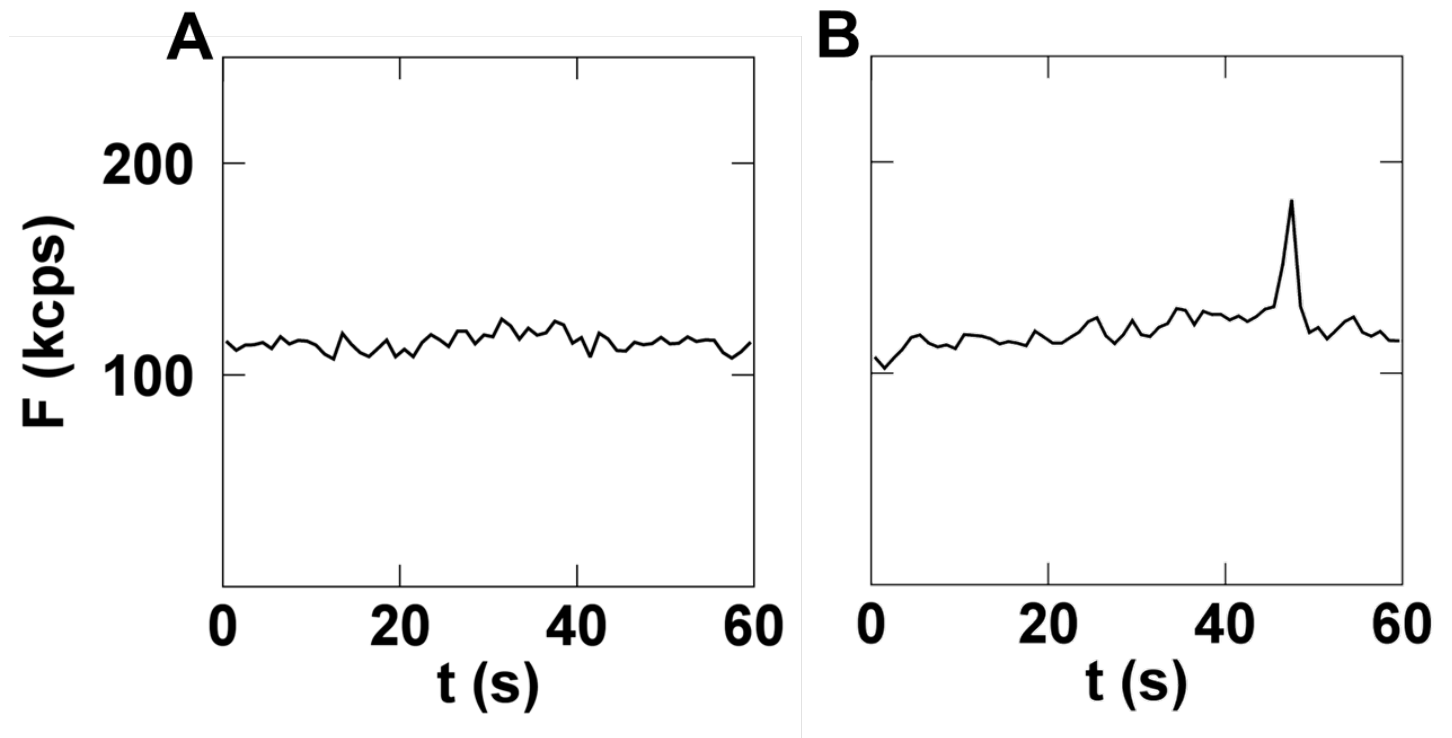


FIGURE 6

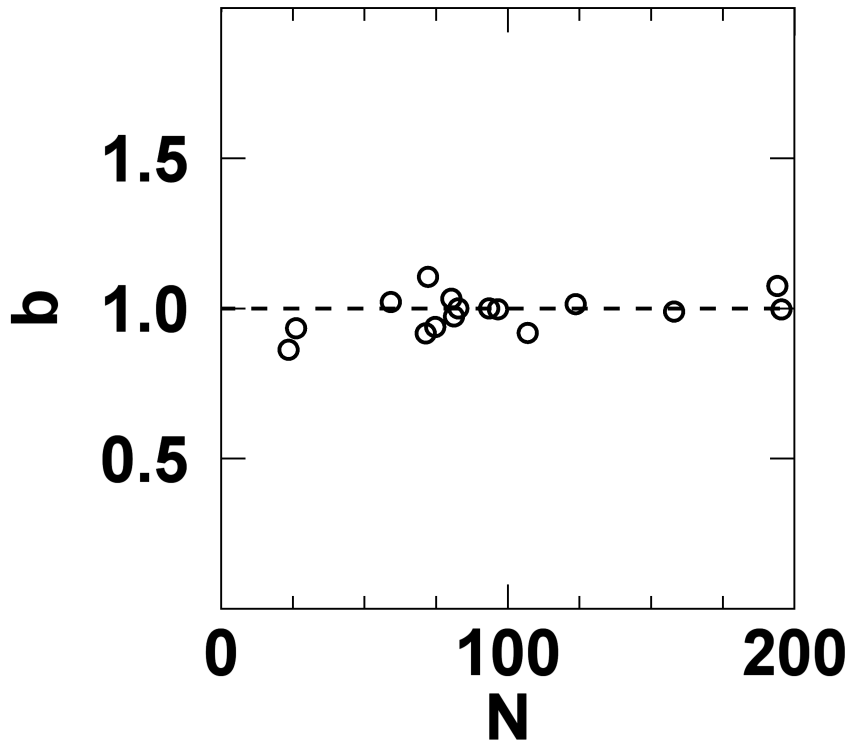


FIGURE 7

